ARTICLES

State-Resolved Dynamics of the CH($A^2\Delta$) Channels from Single and Multiple Photon Dissociation of Bromoform in the 10−20 eV Energy Range†

Viktor Chikan, Frederic Fournier, and Stephen R. Leone*

Departments of Chemistry and Physics, and Lawrence Berkeley National Laboratory, University of California, Berkeley, California 94720-1460

Boris Nizamov

Department of Chemistry & Biochemistry, University of Denver, Denver, Colorado 80208

Received: July 11, 2005; In Final Form: October 12, 2005

Single photon dissociation of bromoform using synchrotron radiation has been investigated by Fourier transform visible fluorescence spectroscopy (FTVIS). The photodissociation of bromoform in the 12−18 eV energy range results in several products, among which are the CH($A^2\Delta$) and CH($B^2\Sigma$) radicals. Vibrational and rotational state distributions of the CH($A^2\Delta$) are determined from their fluorescence spectra. From the threshold photon energy above which emission from the CH($A^2\Delta$) radicals is observed, the most likely process leading to CH(A) formation is $CHBr_3 \rightarrow CH + 3Br$ rather than $CHBr_3 \rightarrow CH + Br + Br_2$. The rotational Boltzmann temperatures in the CH(A → X) emission spectra for $v' = 0$ and $v' = 1$ range between 1570 and 3650 K, depending on the excitation photon energy. From the high rotational excitation, the results suggest that the mechanism for the loss of three bromine atoms is most likely sequential. A small negative emission anisotropy of the CH(A) radicals $[(I_{par} - I_{per})/(I_{par} + 2I_{per}) = -0.024 \pm 0.005]$ is constant across the action spectrum; a small net absorption dipole of $CHBr_3$ in the vacuum ultraviolet is parallel to the 3-fold symmetry axis of the $CHBr_3$ molecule. The state distributions of the CH($A^2\Delta$) radicals from multiphoton dissociation of bromoform using the 266 nm output (three photons) of a femtosecond laser (Boltzmann temperatures: $T^{rot}_{v'=0} = 4250 \pm 300$ K; $T^{rot}_{v'=1} = 3100 \pm 550$ K) are compared to those from the single photon dissociation results (Boltzmann temperatures: $T^{rot}_{v'=0} = 3650 \pm 150$ K; $T^{rot}_{v'=1} = 2400 \pm 200$ K) at the same total excitation energy under collision free conditions. The analysis of the CH(A) rotational populations shows hotter rotational populations for the femtosecond experiment, also suggesting sequential dissociation of the bromoform in the femtosecond experiment. The duration of the femtosecond laser pulse is approximately 180 fs, setting a limit on the time scales for the multiple dissociations.

Introduction

Understanding the dynamics and spectroscopy of highly excited electronic states[1] of radicals and molecules is essential for a variety of practical problems, such as combustion processes[2,3] and discharges.[4] Highly excited electronic states of hydrocarbons are produced by absorption of high energy photons and by high energy collisions with charged and neutral particles present in the interstellar medium and in the upper atmosphere, as well as in plasmas and other high temperature environments. Following the creation of high electronic states, the molecules can undergo photodissociation and dissociative photoionization. These two processes are competitive, and in many cases, it is important to know their relative efficiency, as well as the details of their mechanisms. In the past two decades, several new methods[5] and techniques emerged that allow measurement on the photodissociation dynamics of molecules in the 5−20 eV energy range. Fourier transform infrared spectroscopy (FTIR) is one of these many techniques, which is successfully applied to the dissociation dynamics of small molecules.[6,7] The Fourier transform visible fluorescence spectroscopy (FTVIS) technique used in this study is a simple extension of FTIR spectroscopy into the visible range,[8,9] which allows one to obtain detailed information about the photodissociation dynamics with much higher sensitivity. The high sensitivity of the technique is demonstrated in this study by coupling the FTVIS apparatus with a synchrotron source to study the dissociation dynamics of bromoform in the 10−20 eV excitation energy range.

Bromoform is a common precursor for the CH radical[10−14] by UV photolysis. In many cases, it can be assumed that the dissociation of bromoform is sequential; that is, after absorption of a single photon, bromoform dissociates into $CHBr_2 + Br$, and then, $CHBr_2$ absorbs another single photon, etc. until the CH fragment is produced. However, in some cases (intense field, short pulses), the possibility of simultaneous two or three photon absorption cannot be discounted, and these events could lead

† Part of the special issue "Jürgen Troe Festschrift".
* To whom correspondence should be addressed.

10.1021/jp0538013 CCC: $33.50
Published on Web 12/03/2005

to different fragmentation patterns and dissociation mechanisms. These patterns can also be studied by using single photon excitation with an energy that is twice or three times the energy of a photon used for multiphoton processes. Because of the limited availability of such high-energy tunable photon sources, single photon dissociation mechanisms of bromoform are not well-understood. Upon photoexcitation of bromoform in the VUV energy range, the molecule undergoes fragmentation via several channels, which involve loss of bromine atom(s) or a bromine molecule according to the following schemes:

$$CHBr_3 \rightarrow CHBr_{3-x} + x\ Br \qquad (R1)$$

$$CHBr_3 \rightarrow CHBr_{1-x} + Br_2 + x\ Br \qquad (R2)$$

Many previous photodissociation studies of $CHBr_3$[15−18] were carried out in the 200−300 nm energy range, primarily in the single photon regime. Upon absorption of a single photon in this energy range, a bromine atom or bromine molecule is eliminated from the bromoform. Other groups[8,16,19] investigated the photodissociation of bromoform under more intense laser fields leading to absorption of multiple photons. It was known for a long time that under intense laser fields bromoform yields a considerable amount of CH radical. Lindner et al.[8] investigated the multiphoton dissociation of bromoform at 193 and 248 nm under jet-cooled conditions. The power dependence of their data indicates that absorption of two and three photons can lead to electronically excited CH radicals. The observed CH(A) electronic state may arise from coherent excitation of bromoform or sequential absorption and dissociation processes. Under their conditions, the latter mechanism is favored. Similar conclusions are reached by Liu and Chang,[19] who investigated the photodissociation of bromoform at 266 nm using detection by a frequency-modulated high-resolution spectrometer. In their study, the mechanism involving an electronically excited HCBr intermediate was confirmed.

The goal of the present study is to investigate the photodissociation dynamics of bromoform in the 10−20 eV excitation energy range through the analysis of the internal state distributions of the CH(A) fragment. This work singles out the neutral dissociation channel, but dissociative ionization is also possible.[20] The experiments are carried out using either synchrotron radiation or a femtosecond laser to explore the difference, respectively, between single photon vs multiphoton dissociation dynamics of bromoform. The observed CH(A) rotational distributions, using FTVIS fluorescence detection, suggest that the loss of bromine atoms is sequential in the case of the single photon experiment and also sequential for the multiphoton experiment. The slight emission anisotropy of the CH(A) produced in the single photon case reveals that a net transition dipole of the absorbing state(s) responsible for the dissociation of the CH fragment is located somewhat parallel to the CH molecular axis of bromoform. From the time scale of the femtosecond laser pulse, it is anticipated that the multiphoton photodissociation dynamics takes place on the 100 fs time scale. The present experiment also demonstrates the potential of the basic method to couple the capabilities of FTVIS spectroscopy with synchrotron radiation to understand better the dissociation dynamics of highly excited species in the gas phase.

Experimental Section

UV/vis Fourier transform spectroscopy is a powerful technique to study state-resolved dynamics of photodissociation processes and radical−radical reactions that result in fluorescent molecular fragments, at resolutions not accessible with traditional dispersive units. Figure 1 shows the overview of the experimental apparatus used in this experiment. The experiment consisted of a photodissociation light source between 5 and 30 eV, which was provided by the Advanced Light Source at Beamline 9.0.2 or a frequency-tripled ultrafast laser, in the case of the multiphoton dissociation laser experiment. The light from the Advanced Light Source was a well-collimated synchrotron radiation beam with a 1 mm × 0.3 mm spot at the sample. The photon flux was 10^{14} photons/s with a resolution of 0.1 eV after passing through a monochromator. Before the beam reached the sample, the light passed through a neon or argon gas filter to eliminate the higher harmonics from the undulator. The light source was coupled to a sample cell chamber through two stages of differential pumping. From the typical pressures in the light source (10^{-7} Pa), two apertures and differential pumping constrained the maximum target number density in the cell to be ∼13 Pa. Bromoform was introduced into the cell through a needle valve, and the cell was continuously pumped by a Roots blower in order to eliminate the build up of dissociation products. The action spectra from an earlier setup (with a pulsed valve) and this experiment were identical. If there was product build up, we should have also seen the CH(A) production at lower photon energies, which did not occur. At the end of the cell, a VUV silicon photodiode was used to monitor the intensity of the synchrotron radiation and to measure the absorption spectrum of the bromoform. The cell contained collection optics, which consisted of a spherical mirror and a short focal length lens to maximize the collected light.

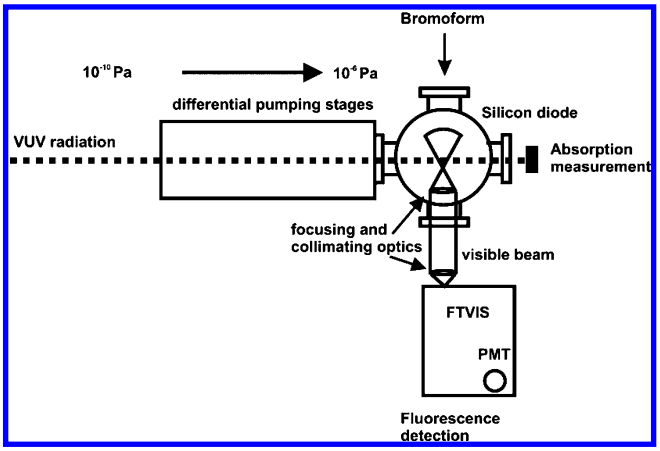

Figure 1. Simplified schematic of the FTVIS apparatus used in this study. The gas is introduced through an effusive source perpendicular to the plane of the schematic at the middle of the vacuum chamber. The synchrotron light path is indicated by a dashed line.

The collected light was collimated and focused onto the UV/vis Fourier transform spectrometer. An iris was placed in front of the spectrometer to reduce the field of view of the instrument; if too large a field of view was used, it could have led to a shift and broadening of the fluorescence spectrum. The light passed through the Michelson interferometer and was imaged onto a photomultiplier (PMT). During alignment, the PMT was used in the photon counting mode; however, during data acquisition, a current-to-voltage amplifier was used. The output of the PMT was then digitized with a 16 bit A/D converter. The resulting interferograms were Fourier transformed to obtain the fluorescence spectra. Typical collection times for one spectrum were 2−4 h. During the collection time, the interferometer was continuously scanning, which minimized the noise associated with slow changes in the experimental conditions (such as decreasing photon flux from the synchrotron light source). The

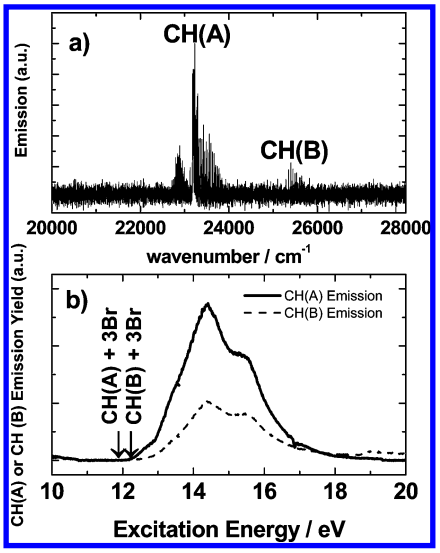

Figure 2. (a) High-resolution spectrum of the CH(A) and CH(B) fluorescence from the photodissociation of the bromoform at 14 eV. The data are collected for 4 h at 1 cm^{-1} resolution. (b) The action spectrum (solid line) of the CH(A) and CH(B) signals was taken with an interference filter in the 10−20 eV excitation energy range. The threshold energies for CH(A) + 3Br and CH(B) + 3Br from bromoform are indicated by arrows in the figure. The pressure of bromoform is 2.6 Pa in both cases.

resulting fluorescence spectra were corrected for the instrument response of the collection optics and the spectrometer. Anisotropy measurements were carried out using a dichroic sheet polarizer in front of the PMT. The reproducibility of the polarizer was checked, and the anisotropy data were corrected for the internal birefringence of the instrument.

The time-resolved experimental apparatus used for the multiphoton dissociation experiments was conceptually the same as the apparatus described above except the synchrotron excitation source was replaced by a femtosecond light source. The femtosecond laser consisted of a mode-locked Ti:Sapphire oscillator pumped by a doubled Nd:YVO_4 continuous laser, delivering 40 fs pulses at 800 nm and 80 MHz. This pulse was amplified via a regenerative amplifier pumped by an intracavity frequency-doubled Nd:YLF laser. The 800 nm pulse was stretched before the amplification and recompressed after, to deliver 50 fs pulses at 1 kHz repetition rate with a power of 2.5 mJ/pulse. The 266 nm femtosecond light used in the time-resolved experiment was produced by sum frequency generation of the frequency-doubled fundamental and the fundamental frequency. The pulse duration of the 266 nm was found to be 180 fs after transport to another room, as determined by a home-built cross-correlator. The 266 nm beam was focused into the interaction chamber with a 10 cm focal length CaF_2 lens to produce power densities of 10^{11} W/cm^2.

The bromoform used in the experiment was commercially available (99% pure) and used without further purification. The bromoform was placed in a Teflon-coated stainless cylinder, and the excess air was removed by pumping on the cylinder.

Results

Synchrotron-Initiated Dissociation of Bromoform. Photodissociation of bromoform in the 10−20 eV energy range results in electronically excited CH radicals and other products. The visible emission spectra of CH(A) and CH(B) from the photodissociation of bromoform at 14 eV are shown in Figure 2a. The action spectra of CH(A) and CH(B) production as a function of photon energy are shown in Figure 2b. These spectra

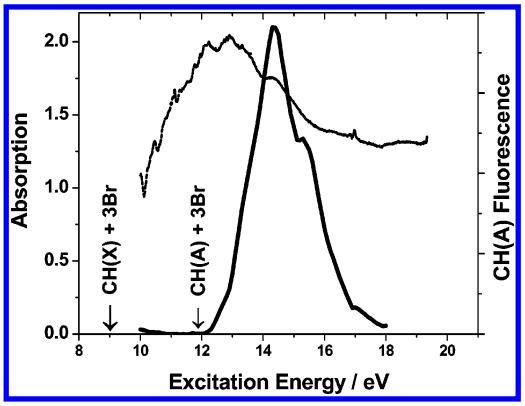

Figure 3. Action spectrum (solid line) of the CH(A) signal was taken with an interference filter in the 10−20 eV excitation energy range. The pressure of bromoform is 2.6 Pa. The absorption spectrum (dashed line) of bromoform is also shown in the figure. The threshold energies for the CH(X) + 3Br and CH(A) + 3Br channels from bromoform are indicated by arrows in the figure.

show very similar behaviors for production of both CH(A) and CH(B). The spectrum shown in Figure 2a was collected at 14 eV excitation energy using the FTVIS spectrometer, while the action spectra shown in Figure 2b were collected using band-pass interference filters. The response function of the FT spectrometer is such that transmission of light at the CH(B) emission wavelength is less than that at the wavelength of the CH(A) emission. Estimating the relative yields of the CH(A) and CH(B) from the fluorescence intensities is somewhat difficult because of predissociation, which changes the intensities of higher rotational levels.[21−23] If the detection system response function, lifetimes, and predissociation rate constants are taken into account, then the corrected action spectra would indicate that the yields for CH(A) and CH(B) are almost the same at this energy. In Figure 2b, the threshold energies required to produce the processes $CHBr_3 \rightarrow$ CH(A) and CH(B) + 3Br are also indicated.

Some information about the importance of the channel producing CH(A) relative to all other channels can be obtained by comparing the absorption spectrum to the action spectrum, shown in Figure 3. The threshold energies for $CHBr_3 \rightarrow$ CH(X) + 3Br and $CHBr_3 \rightarrow$ CH(A) + 3Br are also shown in Figure 3. Figure 3 indicates that bromoform has a strong absorption peak between 10 and 18 eV. If CH(A) is a significant channel, the features observed in the CH(A) action spectrum should also be observed in the absorption spectrum as well. Comparison of the action and absorption spectra shows that the 14.5 eV peak in the action spectrum may show up only as a shoulder in the absorption spectrum; therefore, the channels producing electronically excited CH products may not be the major channels in the photodissociation/photoionization of bromoform. The absorption spectrum of bromoform is dominated by another feature that is red-shifted relative to the main feature in the CH(A) action spectrum, and the entire absorption feature is elevated by a broad continuum. The red-shifted feature could correspond to dissociation channels leading to the formation of CH(X), and other channels, such as $CHBr_2$ + Br, CHBr + 2Br and CHBr + Br_2, all with release of more energy into translational degrees of freedom, could be responsible for the broad continuum absorption. The ionization potential of bromoform is 10.47 eV,[24,25] and some contribution of dissociative photoionization channels to the absorption spectrum is also expected at energies above 10.5 eV.

Figure 4 shows the emission anisotropy of CH(A) with respect to the polarization of the synchrotron radiation along with the

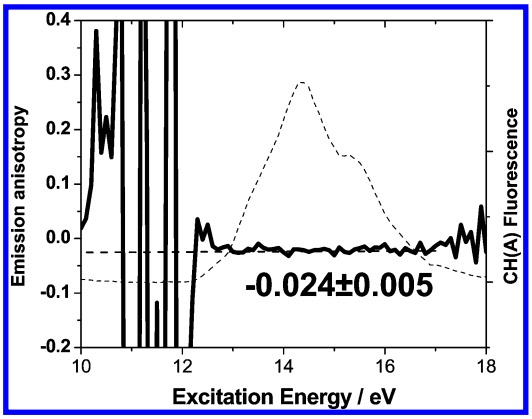

Figure 4. Emission anisotropy (solid line) of the CH(A) fluorescence from the photodissociation of bromoform in the 10−20 eV excitation energy range. The CH(A) action spectrum is also shown in the figure as a reference (dashed line).

previously presented action spectrum of CH(A) from the bromoform photodissociation. The synchrotron output is highly polarized (>99%). The CH(A→X) emission anisotropy is calculated from the fluorescence intensity parallel (I_{par}) and perpendicular (I_{perp}) to the excitation polarization using the following formula.

$$r = \frac{I_{par} - I_{perp}}{I_{par} + 2I_{perp}} \qquad \text{(eq 1)}$$

The anisotropy parameter is a small negative number (−0.024 ± 0.005), which is relatively constant as a function of photon energy across the studied range. The noise in the anisotropy data is directly related to the amount of observed signal, and the data where the CH(A→X) signal is weak are not reliable. The emission anisotropy can usually be related to the relative orientation of the absorption dipole to the emission dipole. However, in this case, multiple dissociation steps are involved between excitation and detection and the result could be more complex.[26]

To address the state-resolved dynamics of the photodissociation of bromoform, several high-resolution spectra of the CH(A) emission are collected for various single photon excitation energies in the 13−15 eV range. The experimental CH(A) spectra normalized to the detection system response function are presented in Figures 5−7. All of the data are taken at 2.6 Pa total pressure, and because the CH(A) fluorescence lifetime is 537 ns, the spectra can be considered nascent. Rotational relaxation rate constants for collisions of CH(A) with bromoform are not available, but considering the rotational relaxation rate constants for collisions of CH with other molecules,[27] at the pressure used here (2.6 Pa), the rotational relaxation is not expected to be significant compared to the fluorescence lifetime.

The experimental spectra are fit to obtain the rotational distributions using the known spectroscopic constants of the CH(X,A) states and a least-squares fitting procedure.[28−30] Before fitting, the spectra are normalized for the response function of the spectrometer and the light collection system. The rotational distributions obtained this way are plotted in Figures 5−7 and are also parametrized using a Boltzmann distribution. The rotational temperatures for the CH($A^2\Delta$, $v' = 0$) vibrational state at 13, 14, and 15 eV excitation energies are 2500 ± 150, 3650 ± 150, and 3600 ± 100 K, respectively. The rotational temperatures for the CH($A^2\Delta$, $v' = 1$) vibrational state at 13, 14, and 15 eV excitation energies are 1400 ± 350, 2400 ± 200, and 3200 ± 400 K, respectively.

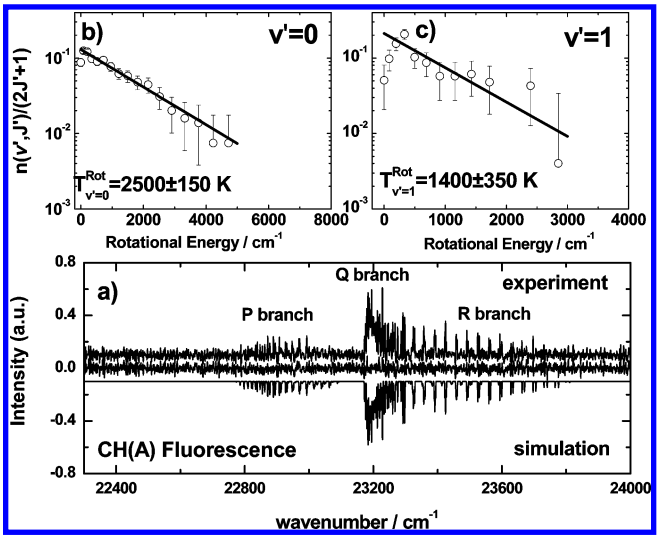

Figure 5. Experimental and simulated spectra of CH(A) from the photodissociation of bromoform at 13 eV excitation energy are shown in panel a. The simulated spectrum is inverted for better visibility. The difference spectrum between the simulation and the experimental spectrum is also shown. The upper graphs show the extracted rotational populations for $v' = 0$ (b) and $v' = 1$ (c) states. The populations are plotted as a function of the available rotational energy. The rotational populations are fitted with a straight line corresponding to a Boltzmann temperature, neglecting the lower rotational states. v' and J' are the corresponding vibrational and rotational quantum numbers.

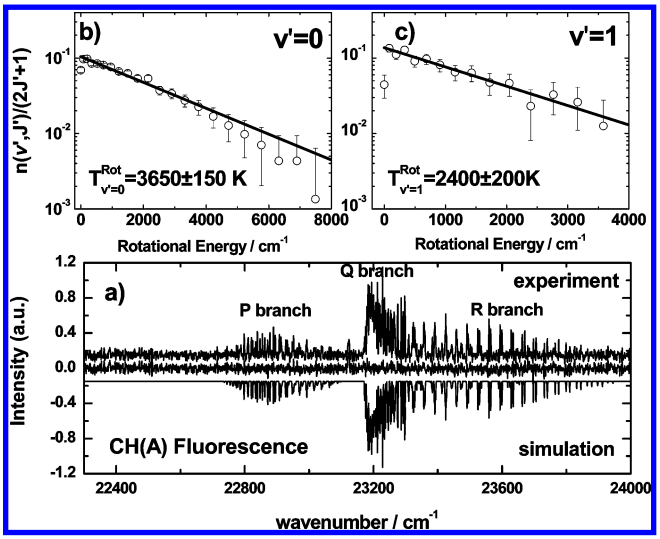

Figure 6. Experimental and simulated spectra of CH(A) from the photodissociation of bromoform at 14 eV excitation energy are shown in panel a. The simulated spectrum is inverted for better visibility. The difference spectrum between the simulation and the experimental spectra is also shown. The upper graphs show the extracted rotational populations for $v' = 0$ (b) and $v' = 1$ (c) states. The populations are plotted as a function of the available rotational energy. The rotational populations are fitted with a straight line corresponding to a Boltzmann temperature, neglecting the lower rotational states. v' and J' are the corresponding vibrational and rotational quantum numbers.

Femtosecond Multiphoton Dissociation of Bromoform. The second portion of this study focuses on understanding the multiphoton dissociation mechanism. Previously, it has been found that the multiphoton photodissociation of bromoform proceeds through multiple intermediates. One goal of these experiments is to compare the dissociation mechanism from the

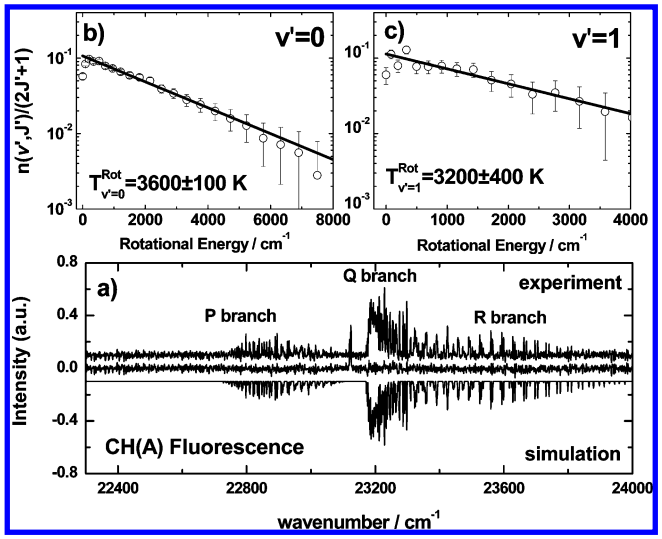

Figure 7. Experimental and simulated spectra of CH(A) from the photodissociation of bromoform at 15 eV excitation energy are shown in panel a. The simulated spectrum is inverted for better visibility. The simulated spectrum is inverted for better visibility. The difference spectrum between the simulation and the experimental spectra is also shown. The upper graphs show the extracted rotational populations for $v' = 0$ (b) and $v' = 1$ (c) states. The populations are plotted as a function of the available rotational energy. The rotational populations are fitted with a straight line corresponding to a Boltzmann temperature, neglecting the lower rotational states. v' and J' are the corresponding vibrational and rotational quantum numbers.

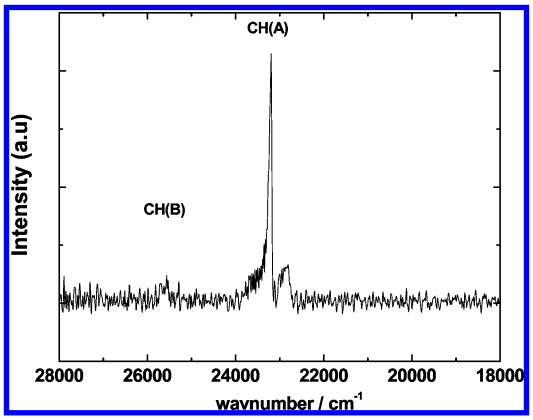

Figure 8. Low resolution (16 cm^{-1}) fluorescence emission of the CH(A) and CH(B) states of the CH molecules from the femtosecond 266 nm multiphoton dissociation of bromoform. The pressure of bromoform is 2 Pa, and the total pressure in the chamber is 13 Pa with the added Ar buffer gas. The duration of the 266 nm femtosecond pulse is 180 fs.

single photon and multiphoton processes at the same excitation energies. The experiment uses the 266 nm output of a femtosecond laser with approximately 180 fs pulse duration to explore the dynamics on time scales similar to the dissociation times of the bromoform. Measurements are made at somewhat higher pressures (13 Pa, mostly Ar) and by time gating the CH(A) emission. On the basis of arguments presented above, the rotational distributions are close to nascent.

Figure 8 shows the emission spectra of the electronically excited products from the femtosecond photodissociation of bromoform at 266 nm, which is assumed to correspond to a three photon energy of 13.96 ± 0.12 eV, to be compared to the single photon data at 14 eV excitation energy. The cubic power dependence of CH(A) from the multiphoton dissociation at low excitation energies suggests that the CH(A) comes from a three photon process. On the basis of previous studies, the three

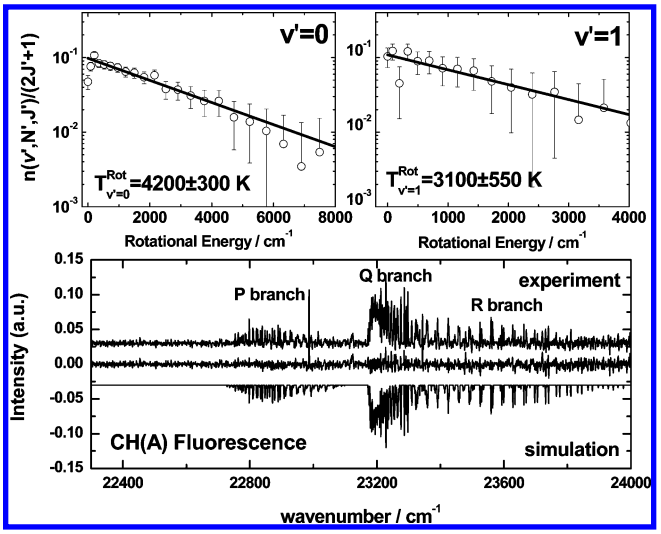

Figure 9. Experimental and simulated spectra of CH(A) from the 266 nm femtosecond multiphoton dissociation of bromoform are shown in panel a. The simulated spectrum is inverted for better visibility. The difference spectrum between the simulation and the experimental spectra is also shown. The upper graphs show the extracted rotational populations for $v' = 0$ and $v' = 1$ states. The populations are plotted as a function of the available rotational energy. The rotational populations are fitted with a straight line corresponding to a Boltzmann temperature, neglecting the lower rotational states.

photon process is also the most likely. If four photons of 266 nm would be absorbed, there would be 4.6 eV of additional energy available. Figure 8 clearly shows that both CH(A) and CH(B) are produced. The experimental spectra show that the relative yield of CH(B) from the single photon experiment is identical to the CH(B) yield from the multiphoton experiment, which strongly suggests that the action spectrum of CH(A) from multiphoton experiment is most likely similar to the action spectrum from the single photon experiment. The experimental data are simulated and fitted to extract the vibrational and rotational population information, as described above. The fractional rotational populations normalized to the rotational degeneracy are shown as a function of the rotational energies in Figure 9 for the multiphoton experiment. The rotational populations are also fitted with a single-exponential representing the Boltzmann temperature. The rotational Boltzmann temperatures for $v' = 0$ and $v' = 1$ are 4300 ± 300 and 3100 ± 550 K, respectively.

Discussion

Two main electronically excited products, CH(A) and CH(B), are observed as a result of a single photon absorption of $CHBr_3$ in the 12−16 eV energy range and also by absorption of three femtosecond photons at 266 nm with a total energy of 13.96 eV. No Br_2 emission could be observed in the single photon experiment. The present study focuses on the channels producing the CH(A) product, which provides important insight into the dynamics of the photodissociation of bromoform.

On the basis of thermodynamic considerations, the CH(A) may be produced through several different channels. The possible channels below 17 eV of excitation energy are listed in Table 1. This study focuses on the CH(A) channels, which are marked in the table. The possibilities are either CH(A) + 3Br or CH(A) + ground or electronically excited Br_2. On the basis of the one-photon onset of the CH(A) fluorescence, the most likely dissociation channel is the CH(A) + 3Br channel. In addition, the CH(X) + 3Br channel may be one of the features in the absorption spectrum. The absorption spectrum indicates

TABLE 1: Energetically Possible Processes from the Photodissociation of Bromoform[a]

reaction	cm^{-1}	eV
$CHBr_3$	0	0
$CHBr_2 + Br$	20461	2.52
$CHBr + Br_2(X)$	27210	3.35
$CHBr + Br_2(A)$	41115	5.07
$CHBr + Br_2(B)$	43112	5.32
$CHBr + 2Br$	43332	5.34
$CHBr + Br_2(C)$	51210	6.32
$CH(X) + Br + Br_2(X)$	56969	7.03
$CH(X) + Br + Br_2(A)$	70874	8.74
$CH(X) + Br + Br_2(B)$	72871	8.99
$CH(X) + 3Br$	73089	9.02
$CHBr + Br_2(D)$	75709	9.34
$CH(A) + Br + Br_2(X)$[b]	80158	9.89
$CH(X) + Br + Br_2(C)$	80969	9.99
$CH(B) + Br + Br_2(X)$	83013	10.24
$CH(C) + Br + Br_2(X)$	88770	10.95
$CH(A) + Br + Br_2(A)$[b]	94063	11.61
$CH(A) + Br + Br_2(B)$[b]	96060	11.85
$CH(A) + 3Br$[b]	96274	11.88
$CH(B) + Br + Br_2(A)$	96918	11.96
$CH(B) + Br + Br_2(B)$	98915	12.21
$CH(B) + 3Br$	99129	12.23
$CH(C) + Br + Br_2(A)$	102675	12.67
$CH(A) + Br + Br_2(C)$[b]	104158	12.85
$CH(C) + Br + Br_2(B)$	104672	12.92
$CH(C) + 3Br$	104886	12.94
$CH(X) + Br + Br_2(D)$	105468	13.02
$CH(B) + Br + Br_2(C)$	107013	13.21
$CH(C) + Br + Br_2(C)$[b]	112770	13.92
$CH(A) + Br + Br_2(D)$	128657	15.88
$CH(B) + Br + Br_2(D)$	131512	16.23
$CH(C) + Br + Br_2(D)$	137269	16.94

[a] The table excludes the possibility that each Br atom can be formed in the ground state [$Br(^2P_{3/2})$] or the first excited state [$Br(^2P_{1/2})$]. [b] Channels that result in production of CH(A).

a broad feature in the 10−16 eV energy range. The onset of this feature agrees well with the CH(X) + 3Br channel. Of course, the assumption is that, upon absorption of a single photon in this energy range, the dissociation would result in CH(X) or CH(A) with high quantum efficiency. This can be inferred indirectly by comparison of the absorption and action spectra (see Figure 3). There is a small shoulder in the absorption spectrum at 14.5 eV, which overlaps with the peak of the CH(A) spectrum and is likely to be assigned to that feature. The absorption of a single photon can also lead to dissociative ionization in this energy range with comparable yields; however, this work only investigates those dissociation channels that result in neutral products.

In addition to CH(A), a significant amount of CH(B) is produced by photodissociation of bromoform in this energy range, as can be seen in Figure 2. The action spectra for production of CH(A) and CH(B) are nearly identical, which can be explained by dissociation with nearly constant branching fractions from the initial state prepared by a single photon absorption in the investigated energy range. The shape of the action spectra in this case is determined by Franck−Condon factors and the competition from other dissociation/ionization processes. Several electronic states may be involved in bromoform to produce absorption in this energy range; however, the nearly constant emission anisotropy data suggest that the major electronic states involved in the production of CH(A) do not change significantly with wavelength. It is possible that the net transition moment is a linear combination of several transition moments, which would lower the emission anisotropy. However, if that is the case, the relative contributions of the different components of the transition moments would most likely be a function of the energy, resulting in energy-dependent emission anisotropy data, which is not observed.

To relate these mechanisms of the dissociation dynamics of bromoform in the single photon experiment to the three photon experiment, the rotational temperatures from the 14 eV synchrotron dissociation experiment can be directly compared to the femtosecond experiment at 266 nm (3×266 nm $= 13.96 \pm 0.12$ eV). The results are summarized in Table 2. Table 2 shows the Boltzmann temperatures for the rotational and vibrational populations. Because the populations of the lower rotational levels deviate slightly from a single Boltzmann distribution, only the populations from higher rotational levels are included in the temperatures on the graphs and in the table. However, in Table 2, the average rotational (and vibrational) energies are calculated by averaging over the experimentally determined populations, rather than by using the temperature derived from the line fit. This is done using the following equations:

$$E_{\mathrm{rot}} = \sum_J f_J E_J \qquad \text{(eq 2)}$$

$$E_{\mathrm{vib}} = \sum_v f_v E_v \qquad \text{(eq 3)}$$

where f corresponds to the normalized fractional population of each rotation or vibration at a particular J or v level and E is the rotational or vibrational energy of the state. The results of the experimental rotational and vibrational energy disposal in the CH(A) from the photodissociation of bromoform are summarized in Table 3. As a reference, the statistical energy distribution is also calculated,[9,31] which assumes the complete randomization of energy among the different degrees of freedom. Deviations from a statistical distribution can be attributed to the dynamics of the system.

Comparison of the values predicted by the statistical calculations and experiment for the vibrational and rotational energy disposal for bromoform photodissociation clearly indicates a nonstatistical behavior. The experimentally observed vibration is always colder, but the observed rotation is hotter at the threshold for CH(A) formation and colder than statistical at higher excitation energies. However, it has to be pointed out that only $v' = 0$ and $v' = 1$ vibrational populations are available since the CH(A) is strongly predissociating at higher vibrational energies. Also, the rotational distributions of the CH(A) at lower J values significantly deviate from a Boltzmann fit, indicating a low population in the low rotational states. On the basis of these observations, it is assumed that the energy distribution is governed by the instantaneous or nearly instantaneous energy release of the dissociating molecule, rather than statistical partitioning. Therefore, a more appropriate model is needed to describe the mechanism of the dissociation. One could envision a process where the internal energy distribution of the fragments is determined by the prompt momentum transfer of breaking bond(s) to the internal degrees of freedom of the fragments without reaching statistical equilibrium. This model would be an impulsive model.[32] The efficiency of the momentum transfer of the breaking bond into the internal degrees of freedom of the fragments depends on the geometry of the molecule. The departing atoms in the breaking bond undergo an inelastic half collision with the rest of the atoms in the molecule. The reduced mass of each molecular fragment and the distance of the impulsive kick from its center of mass determine the efficiency of rotational excitation. Specifically, in the sequential dissocia-

TABLE 2: Experimentally Obtained Rotational and Vibrational Temperatures of CH(A) as a Function of Excitation Wavelength from the Photodissociation of Bromoform[a]

	$T^{rot}_{v'=0}$ (K)	$E^{v'=0}_{rot}$ (cm^{-1})	$T^{rot}_{v'=1}$ (K)	$E^{v'=1}_{rot}$ (cm^{-1})	$N^{vib}_{v'=1}/N^{vib}_{v'=0}$	T^{vib} (K)	E_{vib} (cm^{-1})
13 eV	2500 ± 150	1570 ± 100	1400 ± 350	990 ± 250	0.18 ± 0.01	2400 ± 100	440 ± 20
14 eV	3650 ± 150	2190 ± 100	2400 ± 200	1420 ± 100	0.28 ± 0.01	3300 ± 100	640 ± 20
15 eV	3600 ± 100	2340 ± 50	3200 ± 400	1610 ± 200	0.39 ± 0.01	4500 ± 100	820 ± 20
3 × 266 nm	4250 ± 300	2430 ± 150	3100 ± 550	1600 ± 300	0.28 ± 0.01	3300 ± 100	644 ± 20

[a] The average energies disposed into vibrations and rotations are summarized in cm^{-1}.

TABLE 3: Experimental Average Energies of the CH(A) Vibration and Rotation for Bromoform Photodissociation as a Function of Excitation Wavelength[a]

	E_{avl}	statistical model (cm^{-1})			experiment (cm^{-1})		
	(cm^{-1})	E_{rot}	E_{vib}	E_{trans}	E_{rot}	E_{vib}	E_{trans}
13 eV	9026	1182	748	7095	1480 ± 100	440 ± 20	
14 eV	17126	2195	1758	13172	2000 ± 100	640 ± 20	
15 eV	25226	3208	2767	19249	2250 ± 100	820 ± 20	
3 × 266 nm	16802	2154	1719	12927	2200 ± 100	644 ± 20	

[a] The experimental rotational energies are averaged over $v' = 0$ and $v' = 1$ from Table 2. All results are summarized in cm^{-1}. As a reference,[9] the calculated statistical distributions are also listed assuming complete randomization of energy between the different degrees of freedom.

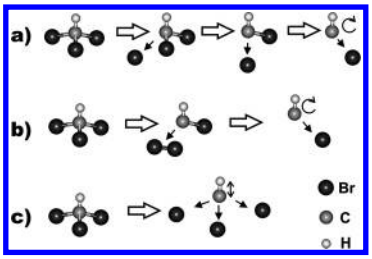

Figure 10. Three possible ways for the photodissociation of bromoform to produce the CH fragment. (a) Three step sequential mechanism resulting in the loss of three bromine atoms. (b) Two step sequential mechanism resulting in the loss of one bromine atom and the bromine molecule. (c) The concerted mechanism resulting in the loss of three bromine atoms. Notice that mechanisms a and b would lead to higher rotationally excited fragments than c.

tion of bromoform, the linear momentum of the first CBr bond breaking would efficiently couple to the rotation of the $CHBr_2$ fragment. Similar conclusions can be reached for the subsequent steps of the sequential dissociation process. The exception is the last step in the sequential process ($CHBr \rightarrow CH + Br$) where the torque on the CH fragment is much smaller because of the small reduced mass of CH and the smaller distance from its center of mass. Another important point of the impulsive energy release is that only certain angular momenta are preferred due to momentum conservation, which would result in rotational distributions peaking at higher J, rather than a simple Boltzmann distribution. This effect can be observed in these experiments, which show less rotational excitation of CH(A) at lower J values; however, this also becomes obscured since multiple steps are involved in the dissociation. Here, the arguments are qualitative only, because the process involves multiple steps, and a quantitative analysis of the impulsive model is rather difficult.

Figure 10 shows a sketch of some possible dissociation mechanisms for $CHBr_3$ by a single photon excitation. There are several extreme possibilities, e.g., a three step sequential (Figure 10a), which results in three bromine atoms; a two step sequential (Figure 10b), resulting in a bromine molecule; and a bromine atom, a fully concerted mechanism (Figure 10c). Close to the threshold energy (13 eV), the average rotational energy is higher than statistical, which shows a preferential disposal into rotation. In a simple dynamical picture, this observation could be interpreted as a result of a sequential dissociation in which the last dissociation step is the dissociation of the bent CHBr intermediate as shown in Figure 10a. The excess energy in rotation can be attributed to the efficient energy transfer to rotation in the final geometry. The difference between experiment and statistical might seem rather small; however, only a small energy release is expected since the impulsive energy release to rotation is rather inefficient because of the relatively small mass of hydrogen as compared to carbon in the CH fragment. At higher excitation energies, both the vibrations and the rotations observed experimentally fall below the statistical values, which could be the result of several factors. At higher excitation energies, electronic excitation of the fragments is also possible. An obvious possibility would be the CH(B) state; however, Figure 2b does not show changes in the relative yield of CH(B) with respect to the CH(A) yield. Another possibility is the electronic excitation of the Br atoms. Up to this point, the assumption is that the bromine atoms are formed in the ground state $Br(^2P_{3/2})$, but the formation of the first excited state $Br(^2P_{1/2})$ is also possible, which lies 3685 cm^{-1} above the ground state. In addition, higher excitation energies would place the molecule at a much higher energy on the repulsive potential, which could result in more efficient impulsive energy release into the translational degrees of freedom.

The results also show that the rotational temperatures are reasonably similar for both the femtosecond experiment and the single photon experiment at similar excitation energies. The femtosecond experiment produces a slightly hotter rotational distribution, which can be understood if it is assumed that both the single photon and the multiphoton experiments proceed through a sequential mechanism, but the single photon dissociation occurs on a faster time scale. A nearly simultaneous "shake off" of the bromine atoms (more concerted, Figure 10c) would result in little (or less) rotational excitation. In the femtosecond experiment, the loss of bromine atoms is most likely sequential, which would lead to intermediate fragments such as CHBr, $CHBr_2$, which are asymmetric compared to the highly symmetric bromoform. These asymmetric species would then easily transfer momentum to the CH(A) fragment, not "feeling" the presence of the other bromine atoms. One would predict that if the laser pulse is shorter, then a coherent excitation of the dissociative state is more likely, as opposed to the sequential dissociation to radicals and further absorption processes. In principle, other mechanisms could also account for the hotter rotational distribution in the femtosecond experiment; one is the alignment of the dipole moment of the bromoform molecule by the laser field or absorption of four or more photons. The former mechanism can be excluded by the following reasons. The typical laser powers for aligning molecules are approximately $\sim 10^{12}$ W/cm^2. In these experiments, the actual laser power is an order of magnitude lower ($\sim 10^{11}$ W/cm^2). Also, the effect of the peak power was briefly explored; it was found that at fixed pulse duration and at three

times less average laser power density, the CH(A) spectrum looks identical to the higher power density data. At fixed average power and longer pulse duration (about 300 fs), the rotational temperature of the CH(A) is slightly higher, which seems to agree well with the concept of a sequential dissociation process. The absorption of four photons is possible, but it is expected that then several other processes could overtake the CH(A)-producing channel, such as dissociative ionization or even dissociation of the CH bond. The inefficient coupling of the electronic states of bromoform to CH(A) is evident in Figure 2b, which clearly shows that at 18.66 eV (four times 266 nm) the CH(A) channel would be highly inefficient. It is possible that the action spectrum of the single photon bromoform dissociation to yield CH(A) could differ from the action spectrum from absorption of multiple photons; however, the power dependence of nanosecond experiments[8] at 193 nm (second order) and at 248 nm (third order) also show good agreement with the single photon action spectrum presented here. In addition, it is apparent from Tables 2 and 3 that the vibrational populations for the single photon and multiphoton experiments are identical, which is not very likely if the total available energy is different in the two experiments.

Conclusion

The photodissociation of bromoform is studied by FTVIS spectroscopy coupled with single photon excitation from a synchrotron source. The study opens up new possibilities to explore the photodissociation dynamics of small molecules using this technique. The observed state-resolved dynamics strongly supports the sequential dissociation mechanism of bromoform. The emission anisotropy data are briefly considered, and further study is under way, which may lead to a better understanding of the dissociating state of bromoform that leads to CH(A). There are many other interesting future investigations possible, such as the breaking of the C_{3v} symmetry (CH_2Br_2, CH_3Br) and effects of the fragment masses (CHF_3, $CHCl_3$, and CHI_3) and how these could alter the dissociation dynamics. The impulsive energy release into CH is somewhat limited by the small reduced mass in the CH fragment about its center of mass, and isotopic substitution of D for H should make the process more sensitive to the rotational dissociation dynamics. Preliminary data indicate that many of the above-mentioned molecules produce CH(A) in this energy range, allowing further investigation of dissociation dynamics in these systems. The experiments are performed at room temperature so the effect of the initial internal energy on the dynamics of the photodissociation process is ignored in this study; however, it is expected to play an important role, which can be investigated in the future. The present method also offers the possibility to study the effect of coherent laser control on the state-resolved photodissociation dynamics of relatively large systems, such as the bromoform molecule.

Acknowledgment. This work has been supported by the U.S. Department of Energy under Contract DE-AC02-05CH11231. We thank all of the staff of the Chemical Dynamics Beamline and particularly John Bozek and Michael Jimenez-Cruz at the Advanced Light Source for their diligent help.

References and Notes

(1) Martinez, T. J.; BenNun, M.; Levine, R. D. *J. Phys. Chem.* **1996**, *100*, 7884.
(2) Osborn, D. L.; Mordaunt, D. H.; Choi, H.; Bise, R. T.; Neumark, D. M.; Rohlfing, C. M. *J. Chem. Phys.* **1997**, *106*, 10087.
(3) Mordaunt, D. H.; Osborn, D. L.; Choi, H.; Bise, R. T.; Neumark, D. M. *J. Chem. Phys.* **1996**, *105*, 6078.
(4) Kalache, B.; Novikova, T.; Morral, A. F. I.; Cabarrocas, P. R. I.; Morscheidt, W.; Hassouni, K. *J. Phys. D: Appl. Phys.* **2004**, *37*, 1765.
(5) Butler, L. J.; Neumark, D. M. *J. Phys. Chem.* **1996**, *100*, 12801.
(6) Woodbridge, E. L.; Ashfold, M. N. R.; Leone, S. R. *J. Chem. Phys.* **1991**, *94*, 4195.
(7) Lin, S. R.; Lin, S. C.; Lee, Y. C.; Chou, Y. C.; Chen, I. C.; Lee, Y. P. *J. Chem. Phys.* **2001**, *114*, 7396.
(8) Lindner, J.; Ermisch, K.; Wilhelm, R. *Chem. Phys.* **1998**, *238*, 329.
(9) Chikan, V.; Leone, S. R. *J. Phys. Chem. A* **2005**, *109*, 10646.
(10) Butler, J. E.; Goss, L. P.; Lin, M. C.; Hudgens, J. W. *Chem. Phys. Lett.* **1979**, *63*, 104.
(11) Butler, J. E.; Fleming, J. W.; Goss, L. P.; Lin, M. C. *Abstr. Am. Chem. Soc.* **1979**, 137.
(12) Butler, J. E.; Fleming, J. W.; Goss, L. P.; Lin, M. C. *Chem. Phys.* **1981**, *56*, 355.
(13) Ren, L.; Kong, F. N. *Chin. Sci. Bull.* **2003**, *48*, 1225.
(14) Zabarnick, S.; Fleming, J. W.; Lin, M. C. *Int. J. Chem. Kinet.* **1989**, *21*, 765.
(15) Huang, H. Y.; Chuang, W. T.; Sharma, R. C.; Hsu, C. Y.; Lin, K. C.; Hu, C. H. *J. Chem. Phys.* **2004**, *121*, 5253.
(16) Zou, P.; Shu, J. N.; Sears, T. J.; Hall, G. E.; North, S. W. *J. Phys. Chem. A* **2004**, *108*, 1482.
(17) Xu, D. D.; Huang, J. H.; Francisco, J. S.; Jackson, W. M. *Abstr. Am. Chem. Soc.* **2002**, *224*, U310.
(18) Bayes, K. D.; Toohey, D. W.; Friedl, R. R.; Sander, S. P. *J. Geophys. Res., [Atmos.]* **2003**, *108*.
(19) Liu, W. L.; Chang, B. C. *J. Chin. Chem. Soc.* **2001**, *48*, 613.
(20) Kishimoto, N.; Matsumura, E.; Ohno, K.; Deleuze, M. S. *J. Chem. Phys.* **2004**, *121*, 3074.
(21) Bauer, W.; Engelhardt, B.; Wiesen, P.; Becker, K. H. *Chem. Phys. Lett.* **1989**, *158*, 321.
(22) Anderson, R. A.; Peacher, J.; Wilcox, D. M. *J. Chem. Phys.* **1975**, *63*, 5287.
(23) Fink, E. H.; Welge, K. H. *J. Chem. Phys.* **1967**, *46*, 4315.
(24) Dixon, R. N.; Murrell, J. N.; Narayan, B. *Mol. Phys.* **1971**, *20*, 611.
(25) Nicholson, D. G.; Rademacher, P. *Acta Chem. Scand. Ser. A: Phys. Inorg. Chem.* **1974**, *A 28*, 1136.
(26) Blokhin, A. P.; Gelin, M. F.; Kalosha, II; Polubisok, S. A.; Tolkachev, V. A. *J. Chem. Phys.* **1999**, *110*, 978.
(27) Cooper, J. L.; Whitehead, J. C. *J. Chem. Soc., Faraday Trans.* **1993**, *89*, 1287.
(28) Baas, R. C.; Beenakker, C. I. M. *Comput. Phys. Commun.* **1974**, *8*, 236.
(29) Bernath, P. F. *J. Mol. Spectrosc.* **1994**, *165*, 301.
(30) Bernath, P. F.; Brazier, C. R.; Olsen, T.; Hailey, R.; Fernando, W.; Woods, C.; Hardwick, J. L. *J. Mol. Spectrosc.* **1991**, *147*, 16.
(31) Muckerman, J. T. *J. Phys. Chem.* **1989**, *93*, 179.
(32) Trentelman, K. A.; Kable, S. H.; Moss, D. B.; Houston, P. L. *J. Chem. Phys.* **1989**, *91*, 7498.